

# Spurious Power Generation in Arm Equivalent Model Variants of Modular Multilevel Converter

Anton Stepanov, Hani Saad, Ulas Karaagac, Jean Mahseredjian

**Abstract**—This paper demonstrates the presence of spurious power generation or losses in the Arm Equivalent Model (AEM) of Modular Multilevel Converters (MMC). Such power is due to numerical effects and can occur if model equations are not solved simultaneously with surrounding power circuit equations, which is the case when the AEM is implemented using control system blocks in an electromagnetic transient simulation software. Depending on operating conditions and simulation parameters, this additional power can represent a significant part of the total converter station losses or even surpass them, thus making simulation results inaccurate.

Several solutions to minimize spurious power generation are proposed, including simulation time-step reduction, extrapolating control signals, including variable resistance into model equations, and ideal voltage source model. Analytical calculations and solutions are validated on a point-to-point MMC-HVDC simulation test case.

**Keywords:** arm equivalent model, HVDC, losses, modeling, modular multilevel converter, simulation.

## I. INTRODUCTION

MODULAR Multilevel Converter (MMC) shown in Fig. 1 is a Voltage Source Converter (VSC) topology that has several advantages in comparison with conventional two- and three-level power electronic converters. Increasing the number of sub-modules (SMs) per arm helps reduce or eliminate filters, improve reliability, and easily achieve scalability to higher voltages. In addition, MMCs have lower losses, lower switching frequency, lower transient peak voltages on IGBTs, and lower switching voltages. During normal operation, the desired AC voltage waveform is constructed by inserting or bypassing the appropriate number of SMs [1].

Due to the increased structural complexity of this type of converter compared to the conventional VSCs, a larger set of models is applicable in electromagnetic transient (EMT) simulations, including detailed model (DM), detailed equivalent model (DEM), arm equivalent model (AEM), and

average value model (AVM) [2]. The choice of the model depends on the given simulated phenomenon and is usually associated with a compromise between required accuracy and tolerable computational burden [3].

The DM representing nonlinear characteristics of IGBTs and diodes offers a very high accuracy. However, this model is the slowest due to the significant number of nodes and nonlinearities [3], [4]. The DEM simplifies the details of the nonlinear characteristics of power switches to only two states (ON and OFF) and uses Thevenin or Norton equivalent circuits to represent each converter arm in the main network equations, which considerably reduces computational burden [4]. The AEM hides individual SM details and deals with a single equivalent capacitor (see Fig. 2). This makes this model advantageous for a large set of grid studies where the converter behavior on SM level is disregarded [5].

The AEM can be implemented in different ways in an EMT-type software: the model equations can be incorporated (hard-code implementation) into the main network equations (MNE). This approach can eliminate the one-time-step delay between the model equations and the MNE. However, the main drawback is the inaccessibility of model equations to the user. Otherwise, the model equations can be implemented using control diagram blocks of the EMT software [6], [7]. In this case, the drawback is the one-time-step delay between the solution of control blocks and MNE in EMT-type software.

In this article it will be analytically demonstrated that in the second approach (model in control blocks), additional spurious power losses can occur, that can affect the overall behavior of the circuit and make the simulation results less reliable. Several solutions to remediate the problem are discussed. Proposed solutions are validated on a practical test case of a point-to-point MMC-based HVDC transmission system.

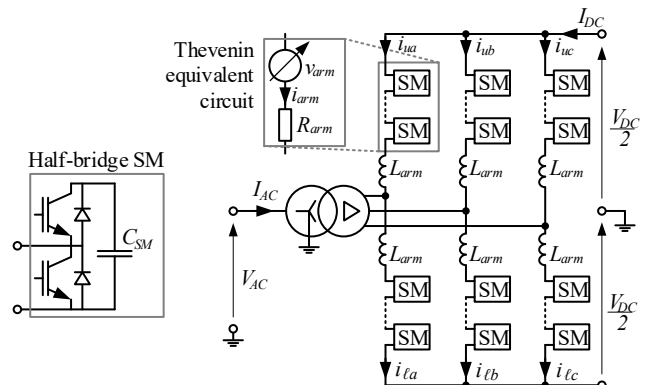


Fig. 1. Three-phase MMC topology with a coupling transformer

This work was supported by the Natural Sciences and Engineering Research Council (NSERC) of Canada as part of the industrial chair “Multi time-frame simulation of transients for large scale power systems.”.

A. Stepanov and J. Mahseredjian are with the Department of Electrical Engineering, Polytechnique Montréal, Montréal, QC, Canada (e-mail of corresponding author: anton.stepanov@polymtl.ca, jeanm@polymtl.ca).

H. Saad is with Réseau de Transport d’Electricité, Paris, France (e-mail: hani.saad@rte-france.com).

U. Karaagac is with the Department of Electrical Engineering, Hong Kong Polytechnic University, Hung Hom, Kowloon, Hong Kong (e-mail: ulas.karaagac@polyu.edu.hk)

## II. NORMAL OPERATION OF ARM EQUIVALENT MODEL

Two operation modes are usually discussed when dealing with MMCs: normal operation and blocked mode. In this paper, normal operation is of primary interest, because power losses are important in steady-state operation [8].

Considering an ideal AEM, i.e. lossless semiconductor devices (no switching or conducting losses), the basic equations of the model for a given arm during normal operation are as follows [2], [9]:

$$v_{arm}(t) = s(t) v_{Ctot}(t) \quad (1)$$

$$i_{Ctot}(t) = s(t) i_{arm}(t) \quad (2)$$

$$\frac{d}{dt} v_{Ctot}(t) = \frac{i_{Ctot}(t)}{C_{eq}} \quad (3)$$

$$C_{eq} = C_{SM} / N_{SM} \quad (4)$$

where  $s$  is the arm switching function,  $v_{arm}$  is the arm voltage,  $v_{Ctot}$  is the equivalent capacitor voltage,  $i_{arm}$  is the arm current,  $i_{Ctot}$  is the equivalent capacitor current,  $C_{eq}$  is the equivalent capacitor,  $C_{SM}$  is the SM capacitance, and  $N_{SM}$  is the number of SMs per arm.

If equations (1)–(3) are solved simultaneously at each time-point, the solution is perfectly accurate, as demonstrated below. Instantaneous arm power on the power circuit side is given by:

$$P_{arm}(t) = i_{arm}(t) v_{arm}(t) \quad (5)$$

Instantaneous power on the equivalent capacitor side becomes:

$$P_{Ctot}(t) = i_{Ctot}(t) v_{Ctot}(t) \quad (6)$$

The powers in (5) and (6) must be equal, because there is no other element that can consume, produce or store energy (as semiconductor losses are not considered in this equation). Considering (2), (6) can be rewritten as

$$P_{Ctot}(t) = i_{arm}(t) s(t) v_{Ctot}(t) \quad (7)$$

When considering (1), (5), and (7) it is clear that  $P_{arm}(t) = P_{Ctot}(t)$ , so no spurious power losses occur irrespective of the waveforms of arm currents and voltages.

Arm equations (1)–(3) can be implemented in an EMT-type simulation software in a form of a control circuit (Fig. 2). Semiconductor conduction losses can be modeled with a constant resistance [1], [2]:

$$R_{arm} = R_{ON} N_{SM} \quad (8)$$

where  $R_{ON}$  is the ON-state resistance of IGBT switches.

In this case, conduction losses can be expressed as

$$P_{COND}(t) = R_{arm} i_{arm}^2(t) \quad (9)$$

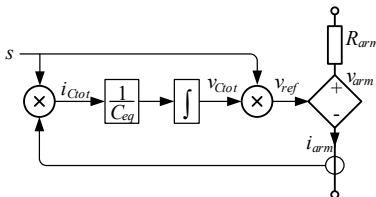


Fig. 2. Classical AEM schematic for normal operation mode.

## III. SPURIOUS LOSSES OF AEM IN STEADY-STATE

In EMT-type software codes it is usual to solve control system equations independently from MNE, which results in a one-time-step delay between the two solutions.

### A. Origin of Losses

The equivalent capacitor  $C_{eq}$  of the AEM can be implemented with control system blocks [6], [7] as shown in Fig. 2. In this case, there is a one-time-step ( $\Delta t$ ) delay between  $v_{ref}$  (reference value from the control blocks), and  $v_{arm}$  (actual voltage):

$$v_{ref}(t) = v_{arm}(t + \Delta t) \quad (10)$$

Considering (10), (1) can be rewritten as

$$v_{arm}(t + \Delta t) = v_{ref}(t) = s(t) v_{Ctot}(t) \quad (11)$$

Considering (11), (7) is rewritten as

$$P_{Ctot}(t) = i_{arm}(t) v_{ref}(t) \quad (12)$$

The difference between  $P_{arm}(t)$  and  $P_{Ctot}(t)$  constitutes the spurious power loss term  $\Delta P$ :

$$\Delta P(t) = P_{arm}(t) - P_{Ctot}(t) \quad (13)$$

Introducing (5), (10), and (12) into (13):

$$\Delta P(t) = -i_{arm}(t) [v_{arm}(t + \Delta t) - v_{arm}(t)] \quad (14)$$

Clearly, as  $v_{arm}$  is not a constant value, the one-time-step delay between controls blocks solution and MNE solution causes a difference between  $P_{arm}(t)$  and  $P_{Ctot}(t)$ , which results in overall spurious power losses or generation (if negative value).

### B. Steady-State Losses

Assuming that simulation time-step is small, the arm voltage derivative at a time-point  $t$  can be approximated by the finite difference:

$$\frac{d}{dt} v_{arm}(t) \approx \frac{v_{arm}(t + \Delta t) - v_{arm}(t)}{\Delta t} \quad (15)$$

With this, (14) can be rewritten to simplify steady-state analysis:

$$\Delta P(t) \approx -\Delta t i_{arm}(t) \frac{d}{dt} v_{arm}(t) \quad (16)$$

For high-power MMCs used for HVDC transmissions it is typical to have high number of levels and circulating current suppression control [10]. In this case, high-frequency components in arm voltages and currents can be neglected, and only DC and fundamental components will be considered in steady-state operation:

$$i_{arm}(t) = I_0 + I_1 \cos(\omega t + \varphi_i) \quad (17)$$

$$v_{arm}(t) = V_0 + V_1 \cos(\omega t + \varphi_v) \quad (18)$$

where  $I_0$ ,  $I_1$ ,  $V_0$ , and  $V_1$  are the amplitudes of the DC and the fundamental components of current and voltage respectively,  $\varphi_i$  and  $\varphi_v$  are the corresponding phase angles, and  $\omega$  is the grid frequency in rad/s.

Considering (18), the arm voltage derivative becomes

$$\frac{d}{dt} v_{arm}(t) = \omega V_1 \cos\left(\omega t + \varphi_v + \frac{\pi}{2}\right) \quad (19)$$

Combining (16), (17), and (19):

$$\Delta P(t) \approx \Delta t \left[ I_0 + I_1 \cos(\omega t + \varphi_i) \right] \omega V_1 \cos\left(\omega t + \varphi_v - \frac{\pi}{2}\right) \quad (20)$$

The above equation can be separated into three harmonic terms: DC component, fundamental component, and double-fundamental-frequency component:

$$\begin{aligned} \Delta P(t) = & \Delta t \omega \frac{V_1 I_1}{2} \cos\left(2\omega t + \varphi_v + \varphi_i - \frac{\pi}{2}\right) \\ & + 2 \Delta t \omega V_1 I_0 \cos\left(\omega t + \varphi_v - \frac{\pi}{2}\right) \\ & + \Delta t \omega \frac{V_1 I_1}{2} \cos\left(\varphi_v - \varphi_i - \frac{\pi}{2}\right) \end{aligned} \quad (21)$$

While undesirable, the presence of oscillating terms will not deteriorate steady-state power balance because all the extra-generated power during one half-cycle will be consumed during the other half-cycle. The constant term, however, is always present and affects the converter power balance.

#### 1) Double-Fundamental-Frequency Spurious Losses

The double-fundamental-frequency components in (21) for the lower arms of phases A, B, and C (denoted as  $\Delta P_2^A$ ) are found from:

$$\Delta P_2^A(t) = \Delta t \omega \frac{V_1 I_1}{2} \cos\left(2\omega t + \varphi_v + \varphi_i - \frac{\pi}{2}\right) \quad (22)$$

$$\Delta P_2^B(t) = \Delta t \omega \frac{V_1 I_1}{2} \cos\left(2\omega t + \varphi_v - \frac{2\pi}{3} + \varphi_i - \frac{2\pi}{3} - \frac{\pi}{2}\right) \quad (23)$$

$$\Delta P_2^C(t) = \Delta t \omega \frac{V_1 I_1}{2} \cos\left(2\omega t + \varphi_v + \frac{2\pi}{3} + \varphi_i + \frac{2\pi}{3} - \frac{\pi}{2}\right) \quad (24)$$

Under balanced conditions, the above three components sum up to zero due to the 120° phase shift in between them. The same formulation applies to the upper arms, so  $\Delta P_2$  has no effect outside of the MMC.

However, depending on control strategies during grid unbalance [10], fundamentals of current and voltage can differ among phases, so it is possible that double-fundamental-frequency spurious losses become visible outside the MMC.

#### 2) Fundamental-Frequency Spurious Losses

The DC components of current and voltage in upper and lower arms are identical in each phase, while the fundamental components have a 180° phase shift. Therefore, the fundamental components of losses in (21) in the lower and upper arm of one phase (denoted as  $\Delta P_1$ ) can be written as:

$$\Delta P_1^{low}(t) = \Delta t \omega V_1 I_0 \cos\left(\omega t + \varphi_v - \frac{\pi}{2}\right) \quad (25)$$

$$\Delta P_1^{up}(t) = \Delta t \omega V_1 I_0 \cos\left(\omega t + \varphi_v + \pi - \frac{\pi}{2}\right) \quad (26)$$

Losses in upper (25) and lower (26) arms cancel each other out, since they are in phase opposition. The same formulation applies to other phases, so there is no effect on the external behavior of the converter even during grid unbalance,

because unbalance between upper and lower arms in each phase is usually kept to a minimum.

#### 3) Constant Spurious Losses

The constant term of (21), is the source of power mismatch affecting the whole grid, which is an overall undesirable behavior. The average value of the spurious losses (denoted as  $\Delta P_0$ ) per arm is given by

$$\Delta P_0 = \Delta t \omega \frac{V_1 I_1}{2} \cos\left(\varphi_v - \varphi_i - \frac{\pi}{2}\right) \quad (27)$$

Depending on the phases of the AC components of arm current and voltage, the losses can be positive as well as negative, i.e. power generation can also occur. In balanced conditions,  $\Delta P_0$  is the same for all six arms, so its effects sum up and can be observed outside of the MMC. During unbalance,  $\Delta P_0$  can differ among arms.

### IV. ELIMINATION OF LOSSES

Four solutions to remove the spurious losses are considered: time-step reduction; extrapolating voltage references (extrapolation AEM); variable resistance AEM; equivalent voltage source AEM.

#### A. Time-Step Reduction

According to (20), spurious power losses in classical AEM depend on  $\Delta t$ , so reducing it will proportionally reduce the losses. Having maximal spurious power losses below or equal 10% of average conduction losses ( $\bar{P}_{COND}$ ) can be considered as satisfactory reduction. In this case, corresponding  $\Delta t$  can be found as:

$$\Delta P \leq 10\% \bar{P}_{COND} \quad (28)$$

$$\Delta t \omega V_1 [I_0 + I_1] \leq 0.1 R_{arm} [I_0^2 + I_1^2 / 2] \quad (29)$$

$$\Delta t \leq 0.1 \frac{R_{arm} [I_0^2 + I_1^2 / 2]}{\omega V_1 [I_0 + I_1]} \quad (30)$$

With this criterion, for high-power HVDC transmissions where voltages are in the order of hundreds of kV and currents are in the order of kA, satisfactory reduction of losses can be achieved with time-steps not higher than 10  $\mu$ s.

#### B. Extrapolation AEM

In steady-state and with relatively small simulation time-steps, arm voltage derivatives do not change significantly between adjacent time-points. This can justify a simple one-time-step extrapolation of the final voltage reference  $v_{ref}^{ext}$  supplied to the controlled voltage source:

$$v_{ref}^{ext}(t) = v_{ref}(t) + \Delta t \frac{d}{dt} v_{ref}(t) \quad (31)$$

$$v_{arm}(t) = v_{ref}^{ext}(t - \Delta t) \quad (32)$$

The reference voltage derivative in (31) can be represented in the vicinity of time-point  $t$  using Taylor series (O represents higher-order terms):

$$v_{ref}(t) = v_{ref}(t - \Delta t) + \Delta t \frac{d}{dt} v_{ref}(t - \Delta t) + O(\Delta t^2) \quad (33)$$

Finally, (14) is rewritten as follows:

$$\begin{aligned} \Delta P(t) &= i_{arm}(t) [v_{ref}^{ext}(t - \Delta t) - v_{ref}^{ext}(t)] \\ &= i_{arm}(t) O(\Delta t^2) \end{aligned} \quad (34)$$

In steady-state and with small time-steps, the second- and higher-order terms  $O(\Delta t^2)$  are considerably smaller than the first-order derivative in (16), therefore  $\Delta P$  is significantly reduced. The derivative of the voltage reference in (31) can be approximated similarly to (15), so:

$$v_{ref}^{ext}(t) = 2v_{ref}(t) - v_{ref}(t - \Delta t) \quad (35)$$

The corresponding implementation is shown in Fig. 3.

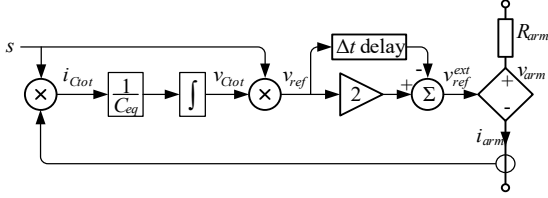


Fig. 3. Extrapolation AEM schematic.

### C. Variable Resistance AEM

Another solution is to include a current-dependent summand in the calculation of arm voltage. Discretization of (3) using trapezoidal integration yields

$$v_{Ctot}(t) = V_{hist\ Ctot}(t) + R_C i_{arm}(t) s(t) \quad (36)$$

with

$$V_{hist\ Ctot}(t) = v_{Ctot}(t - \Delta t) + R_C i_{arm}(t - \Delta t) s(t - \Delta t) \quad (37)$$

$$R_C = 0.5 \Delta t / C_{eq} \quad (38)$$

Multiplying both sides of (36) by  $s(t)$  and considering (1):

$$v_{arm}(t) = R_C s^2(t) i_{arm}(t) + s(t) V_{hist\ Ctot}(t) \quad (39)$$

Since  $V_{hist\ Ctot}(t)$  and  $s(t)$  are known before the solution of MNE at the current time-point, implementation of (39) in the form of a Thevenin equivalent is straightforward:

$$V_{th}(t) = V_{hist\ Ctot}(t) s(t) \quad (40)$$

$$R_{th}(t) = R_C s^2(t) \quad (41)$$

In this case, (1)–(3) are solved simultaneously, so no spurious power losses occur. Equations (36)–(41) can be implemented as shown in Fig. 4. This solution requires refactorization of MNE each time the value of  $R_{th}$  changes.

The trapezoidal integration method is A-stable but prone to numerical oscillations if state variables experience discontinuities. Nevertheless, in this model such oscillations are avoided since the current  $i_{Ctot}$  does not depend on the state variable  $v_{Ctot}$  but is deduced from arm current  $i_{arm}$ .

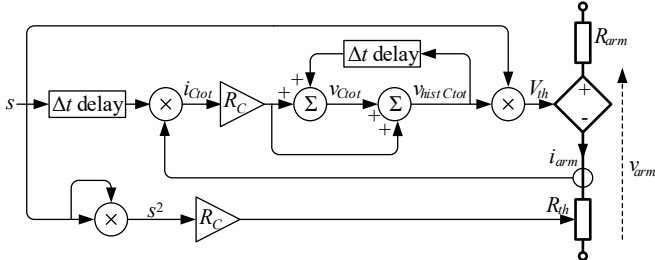


Fig. 4. Variable resistance AEM schematic.

### D. Equivalent Voltage Source AEM

The main drawback of the variable resistance AEM presented in the section IV.C is that it requires MNE refactorization every time the value of  $s$  changes, which can happen at each time-point when  $\Delta t$  is relatively large. To overcome this inconvenience, the voltage drop on  $R_{th}$  can be emulated by an equivalent voltage source  $V_{Req}$  (42). In this case, the MNE matrix does not change so no refactorization is needed.

$$V_{Req}(t) = R_{th} i_{arm}^{ext}(t) \quad (42)$$

where  $i_{arm}^{ext}$  is the extrapolated arm current.

Similarly to (35), extrapolated current can be obtained as:

$$i_{arm}^{ext}(t) = 2i_{arm}(t) - i_{arm}(t - \Delta t) \quad (43)$$

The corresponding implementation is shown in Fig. 5.

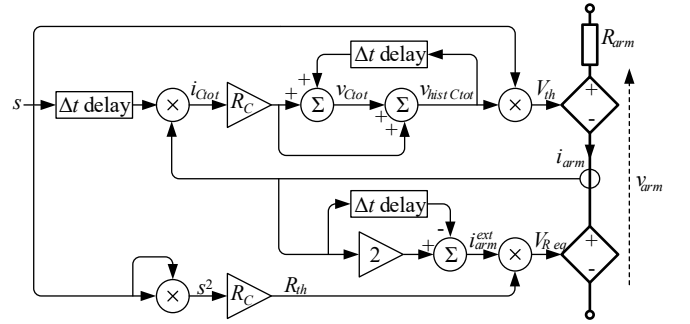


Fig. 5. Equivalent voltage source AEM schematic.

## V. TEST-CASES

A 401-level MMC-based HVDC link (Fig. 6) is used to validate the presented methods for eliminating spurious losses due to one-time-step delay. A standard cascade control system is used [3]. MMC1 controls active and reactive powers, MMC2 controls DC voltage and reactive power. System parameters are given in Table I. DC cable model details can be found in [2]. All simulations are performed in EMTPT [11].

Typically, station transformer losses represent 0.3% of the nominal power of the MMC  $P_{nom}$ . Converter losses are about 0.6% of the nominal power, they represent conduction and switching losses. Another 0.1% can be included for auxiliary and other high voltage equipment [8]. In this study, the total value for the losses represented by arm resistances is taken as 0.6%.

The ON-state resistance  $R_{ON}$  can be found from (44) at nominal power transfer. The obtained value is 2.304 mΩ, which is realistic for high power MMCs [12], [13].

$$0.6 P_{nom} / 100 = 6 N_{SM} R_{ON} [I_0^2 + I_1^2 / 2] \quad (44)$$

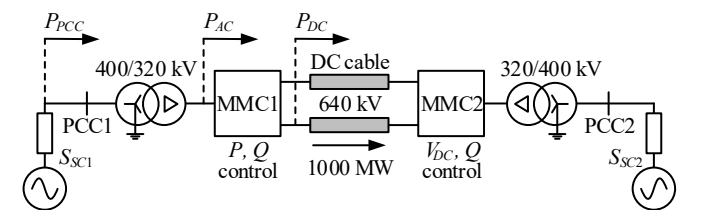


Fig. 6. Simulated point-to-point MMC-HVDC link.

TABLE I  
SIMULATION PARAMETERS

Parameter	Nominal value	Symbol
Simulation time-step	50 $\mu$ s	$\Delta t$
Grid frequency (both grids)	$2\pi \times 50$ rad/s	$\omega$
Grid voltage (both grids)	400 kV	$V_{AC}$
Grid short-circuit level (both grids)	10 GVA	$S_{SC}$
DC voltage	640 kV	$V_{DC}$
Nominal MMC power (both stations)	1000 MW	$P_{nom}$
Number of SMs per arm (HB-SMs)	400	$N_{SM}$
DC voltage reference	1 pu	
Reactive power reference (both stations)	0 pu	
ON-state resistance of IGBTs & diodes	2.304 m $\Omega$	$R_{ON}$
Arm inductance	0.15 pu	$L_{arm}$
Transformer resistance	0.004 pu	
Transformer inductance	0.18 pu	
Capacitor energy	40 kJ/MVA	

### A. Demonstration of Spurious Power Losses

To demonstrate the effects of spurious power losses, active powers at different points of the circuit are shown in Fig. 7 for the case of nominal power transfer using classical AEM: at the point of coupling with the grid ( $P_{PCC}$ ), at the AC terminals ( $P_{AC}$ ), and at the DC terminals ( $P_{DC}$ ) of the converter (see Fig. 6 for the location of these points). DEM is used as a reference model. In addition, adjusted power  $P_{adj}$  is shown in Fig. 7. This is the DC side power compensated for spurious losses:

$$P_{adj}(t) = P_{DC}(t) - \sum_{m,n} \Delta P^{m,n}(t) \quad (45)$$

where  $m = A, B, C$  denotes phases and  $n = up, low$  denotes upper and lower arms.

With both models, the difference between  $P_{PCC}$  and  $P_{AC}$  is 3 MW, which corresponds to transformer losses (0.3% of the nominal power). However, visible difference exists between  $P_{DC}$  values. With the DEM, converter losses amount to approximately 6 MW (difference between  $P_{AC}$  and  $P_{DC}$ ), which corresponds to 0.6% in (44). With the AEM, the losses are considerably smaller. However, adjusted power  $P_{adj}$  is at the same level as  $P_{DC}$  of the DEM, which confirms that spurious losses are the source of the mismatch between  $P_{DC}$ .

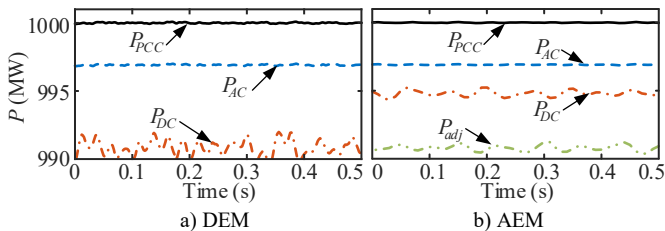


Fig. 7. Transmitted active powers at different points (see Fig. 6).

### B. Validation of Analytical Expression of Losses

To validate the analytical expression of spurious power losses, the HVDC link is subjected to nominal power transfer. The waveforms of  $\Delta P$  in the upper arm of phase A at MMC1 are shown in Fig. 8. Here  $\Delta P_{meas}$  is the measured value from the simulation and corresponds to (13),  $\Delta P_{calc}$  is the

calculated value and corresponds to (21). Also,  $P_{COND}$  is shown in Fig. 8 to demonstrate how unwanted spurious losses compare to the modeled losses. It can be seen that measured and calculated waveforms of  $\Delta P$  match each other well and their values are considerably higher than conduction losses.

Table II shows the amplitudes of  $\Delta P$  harmonics calculated using (22), (25), and (27) for different power angles  $\varphi_{ref}$  at PCC1 (see Fig. 6) terminals. Analytical calculations match simulation results, which validates (21). Same operating conditions are used to demonstrate linear dependency of losses on  $\Delta t$  (see Fig. 9). Measured values (markers) match analytical predictions (lines). Depending on the operation mode, spurious generation can also occur.

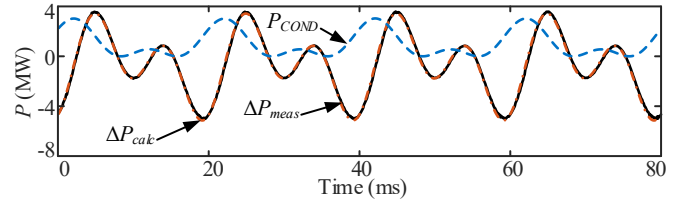


Fig. 8. Power losses in case of nominal power transfer.

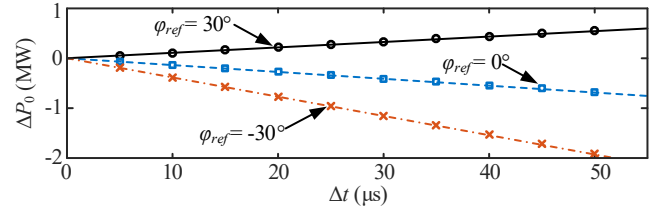


Fig. 9. Effect of time-step on  $\Delta P_0$  in different operating conditions.

TABLE II  
SPURIOUS POWER LOSSES IN DIFFERENT OPERATION MODES (MW)

Operation mode	Measures			Calculations		
	$\Delta P_0$	$ \Delta P_1 $	$ \Delta P_2 $	$\Delta P_0$	$ \Delta P_1 $	$ \Delta P_2 $
$\varphi_{ref} = +30^\circ$	0.56	1.50	2.36	0.54	1.50	2.31
$\varphi_{ref} = 0^\circ$	-0.67	2.15	2.70	-0.69	2.15	2.69
$\varphi_{ref} = -30^\circ$	-1.91	2.18	2.94	-1.93	2.18	2.96

### C. Validation of Proposed Solutions

Validation is performed using the HVDC link in Fig. 6 subjected to nominal power transfer. In the following subsections,  $\Delta P$  and  $P_{COND}$  in the upper arm of phase A at MMC1 are shown to see how spurious losses compare to the desired conduction losses with each solution.

#### 1) Time-Step Reduction

The  $\Delta t$  calculated with (30) is approximately 1.5  $\mu$ s. With this  $\Delta t$ , spurious losses are smaller than conduction losses, but are still visible (see Fig. 10). Their amplitude value is around 200 kW. Besides, the simulation is more than 30 times slower.

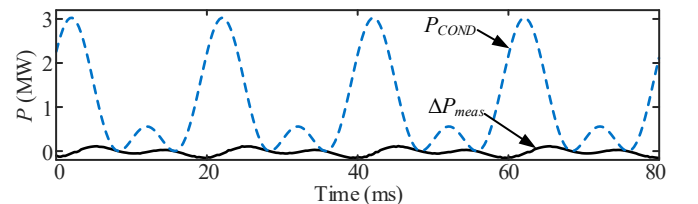


Fig. 10. Power losses with  $\Delta t = 1.5 \mu$ s.

### 2) Extrapolation AEM

A one-time-step linear extrapolation is applied to the variable voltage source reference, as per section IV.B. Results are shown in Fig. 11. In this case,  $\Delta P$  is smaller than in the case of Fig. 10 but due to higher-order terms in (34) spurious losses are not exactly zero (around 100 kW).

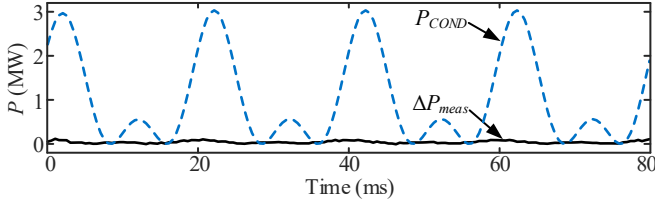


Fig. 11 Power losses with extrapolation AEM.

### 3) Variable Resistance AEM

Variable resistance AEM is implemented as explained in section IV.C, results are shown in Fig. 12. With variable resistance,  $\Delta P$  is in the order of  $10^{-7}$  W, which is negligible. Thus, this model achieves the highest possible accuracy.

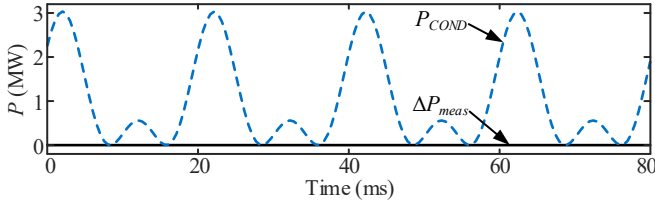


Fig. 12 Power losses with variable resistance AEM.

### 4) Equivalent Voltage Source AEM

Equivalent Voltage Source AEM is implemented as explained in section IV.D, results are shown in Fig. 13. In this case, spurious losses are below 1 kW, which is also negligible if compared to  $P_{COND}$ .

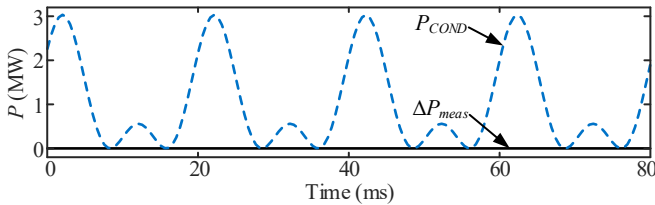


Fig. 13 Power losses with equivalent voltage source AEM.

## VI. CONCLUSIONS

This article demonstrates that spurious power loss or generation can occur when using the arm equivalent model of MMC implemented in an EMT-type simulation software using control blocks. This is caused by the delay between solutions of power circuit and control system equations. Depending on the simulation conditions, such spurious power can represent a significant part of or even exceed total station losses, thus jeopardizing the accuracy of the simulations.

Analytical formulation of spurious losses is developed and validated in this paper. Several solutions to remove such losses are proposed, and their effects are demonstrated on a point-to-point MMC-HVDC link. All solutions reduce spurious power to acceptable values. Variable resistance AEM

is the most accurate solution and eliminates spurious power completely but requires refactoring MNE each time the value of arm switching function changes. Emulating the effect of the variable resistance with an equivalent voltage source AEM eliminates the need to refactor MNE on the expense of slightly increasing spurious power (below 1 kW). Extrapolation AEM requires minimal implementation efforts but remaining spurious power is higher (100 kW). Time-step reduction is the easiest solution but requires very small time-steps to considerably reduce spurious power. The presented solutions could also be applicable to other multilevel converters, such as cascaded multilevel converter.

## VII. REFERENCES

- [1] H. Saad, "Modélisation et simulation temps réel d'une liaison HVDC de type VSC-MMC," Ph.D. Thesis, Département de génie électrique, Polytechnique Montréal, Montreal, Canada, 2015.
- [2] H. Saad, S. Denetière, J. Mahseredjian, P. Delarue, X. Guillaud, J. Peralta, and S. Nguefeu, "Modular Multilevel Converter Models for Electromagnetic Transients," *IEEE Trans. on Power Delivery*, vol. 29, pp. 1481-1489, June 2014.
- [3] J. Peralta, H. Saad, S. Denetière, J. Mahseredjian, and S. Nguefeu, "Detailed and Averaged Models for a 401-Level MMC-HVDC System," *IEEE Trans. on Power Delivery*, vol. 27, pp. 1501-1508, July 2012.
- [4] H. Saad, J. Peralta, S. Denetière, J. Mahseredjian, J. Jatskevich, J. A. Martinez, A. Davoudi, M. Saeedifard, V. Sood, X. Wang, J. Cano, and A. Mehrizi-Sani, "Dynamic Averaged and Simplified Models for MMC-Based HVDC Transmission Systems," *IEEE Trans. on Power Delivery*, vol. 28, pp. 1723-1730, July 2013.
- [5] N. Ahmed, L. Angquist, S. Norrga, A. Antonopoulos, L. Harnefors, and H.-P. Nee, "A Computationally Efficient Continuous Model for the Modular Multilevel Converter," *IEEE Journal of Emerging and Selected Topics in Power Electronics*, vol. 2, pp. 1139-1148, Dec. 2014.
- [6] H. Saad, K. Jacobs, W. Lin, and D. Jovcic, "Modelling of MMC including half-bridge and Full-bridge submodules for EMT study," *19th Power Systems Computation Conference, PSCC 2016*, Genova, Italy, June 2016, pp. 1-7.
- [7] N. Ahmed, L. Ångquist, S. Norrga, and H.-P. Nee, "Validation of the continuous model of the modular multilevel converter with blocking/deblocking capability," *10th IET International Conference on AC and DC Power Transmission (ACDC 2012)*, Birmingham, UK, Dec. 2012, pp. 1-6.
- [8] IEC International Standard, "Power losses in voltage sourced converter (VSC) valves for high-voltage direct current (HVDC) systems – Part 2: Modular multilevel converters", 115 p., 2014
- [9] S. Norrga, L. Angquist, K. Ilves, L. Harnefors, and H. P. Nee, "Decoupled steady-state model of the modular multilevel converter with half-bridge cells," *6th IET International Conference on Power Electronics, Machines and Drives (PEMD 2012), 27-29 March 2012*, Stevenage, UK2012, pp. 1-6.
- [10] A. Stepanov, H. Saad, J. Mahseredjian, and A. Wataré, "Overview of Generic HVDC-MMC Control under Unbalanced Grid Conditions," *International Power Systems Transients Conference (IPST 2017)*, Seoul, South Korea, June 2017, pp. 1-6.
- [11] J. Mahseredjian, S. Denetière, L. Dubé, B. Khodabakhchian, and L. Gérin-Lajoie, "On a new approach for the simulation of transients in power systems," *Electric Power Systems Research*, vol. 77, pp. 1514-1520, Sep. 2007.
- [12] CIGRE Working Group B4.57, "Guide for the Development of Models for HVDC Converters in a HVDC Grid", 221 p., 2014
- [13] S. Denetière, "Contributions à la modélisation et à la validation des modèles de liaisons HVDC de type VSC-MMC dans les outils de simulation temps réel," Ph.D. Thesis, Département de génie électrique, Polytechnique Montréal, Montreal, Canada.